Mechanical Response of Carbon Nanotubes under Molecular and Macroscopic Pressures

Jonathan R. Wood,[†] Mark D. Frogley,[‡] Erwin R. Meurs,[†,§] Andrew D. Prins,[‡] Ton Peijs,[||] David J. Dunstan,[‡] and H. Daniel Wagner*[,†]

Department of Materials and Interfaces, Weizmann Institute of Science, Rehovot 76100, Israel, Department of Physics, Queen Mary and Westfield College, University of London, London E1 4NS, U.K., Department of Materials, Eindhoven University of Technology, Eindhoven, The Netherlands, and Department of Materials Science and Engineering, Queen Mary and Westfield College, University of London, London E1 4NS, U.K.

Received: June 25, 1999; In Final Form: September 6, 1999

High hydrostatic pressures were applied to single-wall carbon nanotubes by means of a diamond anvil cell (DAC), and micro-Raman spectroscopy was simultaneously used to monitor the pressure-induced shift of various nanotube bands. The data confirm recent results independently obtained from internal pressure experiments with various liquids, where the peak shifts were considered to arise from compressive forces imposed by the liquids on the nanotubes. It is also shown that the nanotube peak at 1580 cm^{-1} (the G band) shifts linearly with pressure up to 20 000 atm and deviates from linearity at higher pressure. This deviation is found to be coincident with a drop in Raman intensity for the disorder-induced peak at 2610 cm^{-1} (the overtone of the D* band), possibly corresponding to the occurrence of reversible flattening of the nanotubes. The independent results presented here confirm the potential of nanotubes as molecular sensors.

Introduction

Experimental and theoretical results[1−6] suggest that carbon nanotubes hold promise as reinforcement materials for nanocomposites. Their use as nanosensors though has so far been overlooked. Here, we demonstrate the potential of single-wall carbon nanotubes (SWNTs) as molecular and macroscopic sensors.

The disorder-induced Raman band (D* band) reflects a breathing vibrational mode in graphite.[7] Embedding SWNT bundles in a polymer shifts the D* band peak with respect to its position in air. This shift in Raman wavenumber was originally attributed to a transfer of shrinkage and thermal stresses to the tubes from the surrounding polymer.[8] More recently, however, it has been determined that only part of the shift can be attributed to thermal strains, while the remainder of the shift is a consequence of the internal pressure of the medium.[9] This was shown by placing nanotubes in a range of liquids and performing a Raman spectroscopic scan (Renishaw Ramascope, He−Ne laser, 632.8 nm, 1 mW) on the aggregate particles suspended in the liquid and also on a composite of nanotubes embedded in a polymer matrix. As the wavenumber of the peak increases upon immersion and embedding, the tubes are under compression. The D* band possesses A_{1g} vibrational symmetry, the frequency of which is only weakly dependent on nanotube diameter.[10,11] A_{1g} vibrational symmetry may be related to breathing modes whose vibrations are in the radial direction and/or related to breathing modes along the nanotube axis.[12] Peak shifts were found[9] to be significantly different for the liquids used, and these results are summarized in the present article for direct comparison with pressure measurements. In this paper we confirm that the shift of the D* peak is a result of pressure using a diamond anvil cell (DAC). We also present the shifts of the peak at 1580 cm^{-1} (G band), and comparisons are made with peak shifts obtained utilizing thermal strains by embedding nanotubes in a polymer matrix.

The two spectral features of interest here are the D* peak (2610 cm^{-1} in air) and the G band (1580 cm^{-1} in air). The peak at 1580 cm^{-1} has been identified tentatively with an unresolved triplet containing three modes (A_{1g}, E_{1g}, E_{2g}).[10] In graphite the peak centered at 1580 cm^{-1} has been identified as an E_{2g} (stretching) mode.[11,13] The peaks in the 1500−1600 cm^{-1} region are often referred to as tangential modes because they are associated with the C−C stretching of SWNTs in the tangential direction.[10,14] In this paper we show the effect of hydrostatic pressure applied to nanotube aggregates and compare it with results from simple immersion of the nanotubes in various liquids. The use of direct macroscopic pressure in the DAC allows the simple manipulation of the nanostructures for comparison with peak shifts derived from internal pressures of immersion media. The shifts of the D* band for the liquid and pressure experiments are presented together to show that the nanotubes act as molecular sensors. In addition, the shift of the nanotube peak at 1580 cm^{-1} is also presented, showing a linear dependence with hydrostatic pressure up to 2000 MPa. Finally, experimental results for nanotubes embedded in a polymer matrix are presented and discussed.

Nanotubes in Liquids

The cohesive energy density and the internal pressure are interchangeable parameters, similar to the energies or forces at the surface of liquids, which describe the powerful cohesive forces that hold liquids together.[15,16] A balance between attractive and repulsive molecular forces exists in the interior of a liquid, which, if disturbed by a second phase (in this case the nanotube aggregates), induces the transfer of a large hydrostatic stress from the surrounding liquid to the suspended particles. The magnitude of this stress can be determined from

[†] Weizmann Institute of Science.
[‡] Department of Physics, Queen Mary and Westfield College.
[§] Eindhoven University of Technology.
[||] Department of Materials Science and Engineering, Queen Mary and Westfield College.

10.1021/jp992136t CCC: $18.00
Published on Web 11/04/1999

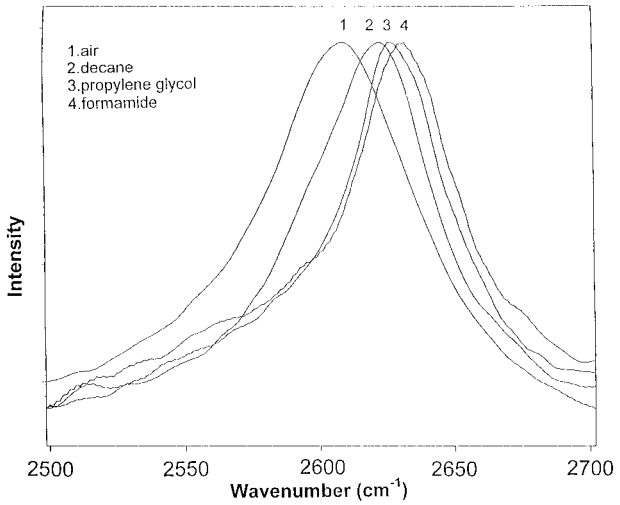

Figure 1. Effect of immersion of SWNT aggregates on the frequency of the D* band in the Raman spectrum. Placing the nanotubes in the liquids increases the wavenumber of the peak position compared to that in air. The intensity has arbitrary units.

the energy of vaporization ΔE_v (J/mol) and the molar volume of the liquid V (cm^3/mol), the thermodynamic quantities that describe the attractive strength between molecules. Values of the cohesive energy density (CED) can be calculated from the enthalpy of vaporization ΔH_v (J/mol) or from the solubility parameter δ ($(J/cm^3)^{1/2}$ or $MPa^{1/2}$) of the liquid, using the relation[16]

$$\mathrm{CED} = \delta^2 = \frac{\Delta E_v}{V} \approx \frac{\Delta H_v - RT}{V} \qquad (1)$$

where T (K) is the temperature and R (J/molK) is the universal gas constant. The cohesive energy density has the units of pressure or stress.

Figure 1 shows the Raman shifts for single-wall nanotubes immersed in three liquids compared to the peak position in air at room temperature and pressure. Under normal conditions the external pressure (1 atm) is small compared with the internal pressure and has little effect, so the shift in Figure 1 is purely a consequence of the liquid media. The nanotubes are apparently responding to intermolecular forces in the liquid. It was anticipated that application of high external pressures could be used to increase the internal pressure.

Diamond Anvil Cell Experiments

Pressure was applied at room temperature in a Dunstan-type miniature diamond anvil cell (DAC),[17] using condensed argon as a pressure medium. The pressure was determined by the ruby fluorescence method, which is accurate to within 100 MPa up to pressures of 20 GPa.[18] Several flakes of SWNT aggregate, approximately 150 μm × 150 μm in size and a few micrometers thick were stacked in the cell alongside the ruby chip. Raman spectra were recorded at several pressures using a few milliwatts of 632.8 nm laser light focused to a ~10 μm diameter spot on the sample. A long working distance objective (numerical aperture of 0.35) was used with the Ramascope for efficient light collection from the DAC.

Figure 2 shows the plot of peak position for the D* peak from the DAC experiments and for all the liquids tested against their respective cohesive energy density.[16] It can be seen that there is a strong concordance between the two data sets. A trend similar to that in Figure 2 can be obtained for the surface tension of the liquid γ_l instead of the CED by plotting the wavenumber against $\gamma_l(1/V)^{1/3}$, in agreement with the semiempirical relation between these two parameters.[19] Although it is anticipated that the argon medium also has internal pressure acting on the nanotubes, this is expected to be negligible, since the intermolecular interactions in liquid argon are very small.

It was also noted that the intensity of the D* peak obtained from the DAC experiments dropped between 1000 and 1800 MPa and could not be measured at pressures above 2200 MPa (Figure 3). The signal was recovered upon subsequent reduction of the pressure below 2000 MPa as discussed later. This drop in intensity was also noted with the liquid data in that the spectra from nanotubes immersed in water were considerably weaker than liquids with lower cohesive energy densities.

Figure 4 shows the pressure dependence of the G band, initially at 1580 cm^{-1} in air. In contrast to the D* peak (Figure 2) the shift is linear up to about 2000 MPa (~20 000 atm). However, the G band is mostly masked when used in a liquid.

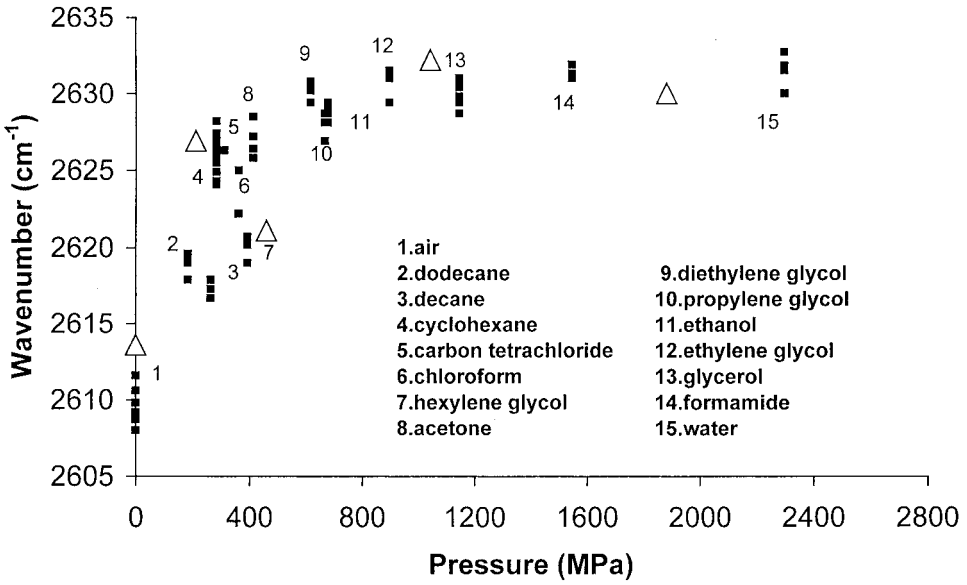

Figure 2. Frequency shift of D* band in the Raman spectrum on immersion of SWNT aggregates in liquids of various cohesive energy densities. The triangles show the pressure data from the DAC experiments.

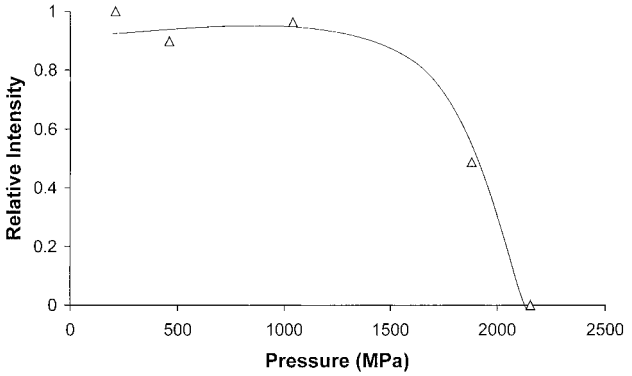

Figure 3. Relative intensity of D* band with respect to the Raman spectrum of diamond.

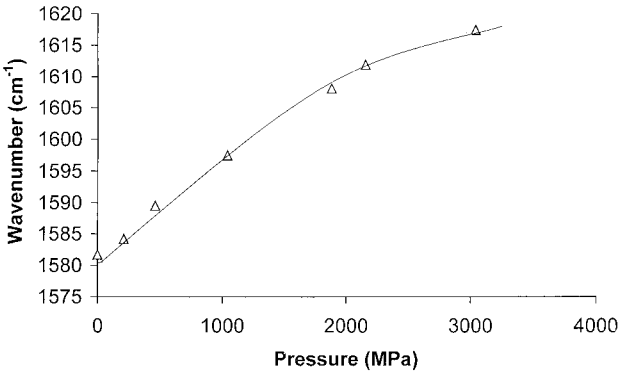

Figure 4. Frequency shift of G band in the Raman spectrum with hydrostatic pressure from the DAC.

Nanotubes in Polymer

SWNTs were also embedded in a polycarbonate matrix. The polymer was first dissolved in methylene chloride, and the nanotubes were dispersed in a large volume of ethanol and briefly sonicated in order to break up the aggregates. The polymer solution was mixed with the nanotube dispersion, producing a clear liquid. The solvents were evaporated, and the gray crystalline residue was pressed in a hot press at a temperature above the crystalline melting point of polycarbonate (245 °C). The resulting pressed sheet also had a dark-gray appearance and was found to be amorphous and have a glass transition temperature (T_g) of 150 °C (423 K) from DSC measurements, in accordance with literature values for unmodified polycarbonate.[20] The pressed sheet was placed in a hot stage on the Raman spectrometer, and carbon nanotube spectra were recorded at incremental temperatures from liquid nitrogen temperatures to above the T_g of the polymer.

Figure 5 shows the relationship between the D* peak position and the equilibrium temperature where a significant shift in peak position can be observed as the temperature is decreased from the glass transition temperature. It should be noted that the peak position at this stress-free temperature does not equal the peak position of SWNT in air. This corroborates the previous observations with liquids that the mere presence of a secondary phase around the nanotubes is sufficient to cause a significant shift. Although there is a small temperature dependence of peak position for SWNT in air over the temperature range investigated,[8] the magnitude of the shift for SWNT in polycarbonate at the glass transition temperature can be explained by examining the CED of the polymer.

The thermodynamic enthalpy of vaporization term is not meaningful for polymers because of their involatility, but the CED of polymer systems can be estimated from the solubility

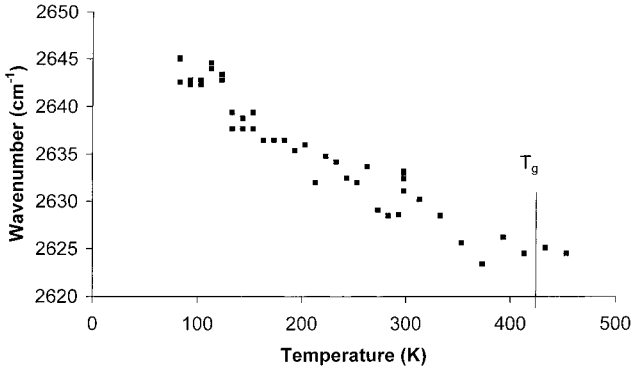

Figure 5. Relationship between D* band position and temperature. Note that the wavenumber is relatively constant around the T_g of the polymer.

parameter of a solvent that dissolves the polymer or from molar attraction constants. By use of Small's molar attraction constants[21] for the polycarbonate repeat unit, the cohesive energy density is 385 MPa, which gives a solubility parameter of 19.6 $MPa^{1/2}$. This is similar to the solubility parameter for methylene chloride ($\delta = 19.8$),[16] which was the organic liquid used in the aforementioned solution procedure. From Figure 2 the calculated value of the cohesive energy density of SWNT in polycarbonate gives a peak position of between 2620 and 2627 cm^{-1}, the position corresponding to nanotubes embedded in the unstressed polymer. This is very similar to the peak position observed for polycarbonate at the glass transition temperature (Figure 2), where the thermal stress component is zero.

The shift of the D* band for the embedded nanotubes is therefore a consequence of the internal pressure, which is relatively invariant with temperature (eq 1) and the thermal strain that is transferred from the surrounding polymer to the nanotubes. Assuming that the thermal strain in the polymer matrix is equal to the thermal strain in the embedded nanotubes and that the thermal expansion coefficient of the polymer matrix α_m is much greater than that of the carbon nanotube α_{NT}, it is possible to construct a relation between the thermal strain and the Raman shift, using

$$\epsilon = (\alpha_m - \alpha_{NT})\Delta T \approx \alpha_m \Delta T \qquad (2)$$

where ΔT is the difference in temperature between the glass transition temperature (where the thermal stress is zero) and the ambient temperature. The parameter α_m, which has a small temperature dependence for polymers below their glass transition temperatures, was considered as a constant and had a value of $65 \times 10^{-6}\ K^{-1}$, which is the literature value for polycarbonate. Figure 6 shows the relation between thermal strain and Raman wavenumber.

Discussion

With the position of the D* band calibrated with respect to strain from the thermal strain experiments and with respect to pressure from the cohesive energy density experiments, it is possible to construct the compressive stress−strain relation for SWNT. By use of the relation for a close-ended cylinder, $\sigma = pR/(2t)$, where σ is the stress in the axial direction, p is the pressure, and R and t are the radius and thickness of the nanotube, respectively, the stress in the nanotube can be determined. Transmission electron microscopy was used to measure the diameter of the SWNTs ($d = 1.1$ nm), and a wall thickness value of 0.066 nm was taken from Yakobson et al.[22]

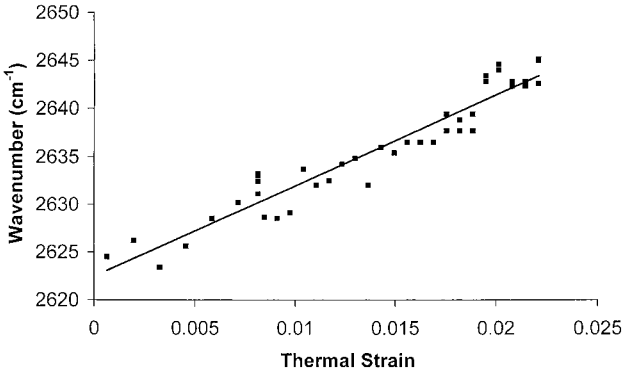

Figure 6. Relationship between D* band position and thermal strain as calculated from eq 2 for SWNT embedded in polycarbonate. The linearity of the plot supports the strain identical assumption, and the intercept value (2622.5 cm^{-1}) demonstrates that at zero thermal strain there is a shift of 12.5 cm^{-1} with respect to the position in air (2610 cm^{-1}). The temperature dependence of the wavenumber of the nanotubes themselves is no more than 4 cm^{-1} over the temperature range investigated.[8]

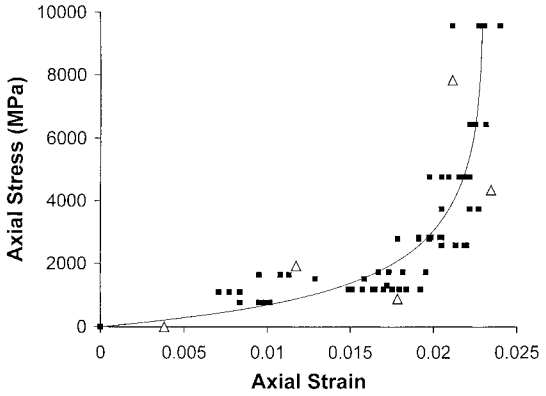

Figure 7. Compressive stress−strain curve for SWNT determined from the two calibration graphs (Figures 2 and 6). Triangles show the data from the DAC experiments, squares are from the experiments on liquids.

Figure 7 shows the compressive stress−strain curve using the liquid and pressure data from Figure 2. Both data sets are strikingly similar, even though the methods of inducing pressure (and thus the spectral shifts from which Figure 7 is derived) are very different. It is apparent that the modulus is not a unique value but increases with increasing strain. This is similar to the behavior of elastomers in compression,[23] which are also network structures. The shape of the curve is not unexpected when it is considered that SWNT have high moduli despite being highly flexible. The compressive modulus ranges between 100 GPa at low strains to about 5 TPa at high strains. This could explain the scatter in the data of Krishnan et al.,[24] since slightly different applied strains can yield large differences in Young's modulus. Interestingly, Yakobson et al.[22] predicted a Young's modulus of 5.5 TPa using this wall thickness (0.066 nm) in molecular dynamics simulations. This is very close to the high strain modulus value (5 TPa) in Figure 7. It is also possible to use the graphite interlayer distance (0.34 nm) instead of Yakobson's wall thickness (0.066 nm) to derive the axial stress; this does not change the shape of the curve but does reduce the moduli. The high strain modulus values remain in the terapascal range.

The G band was not found to move in the polymer experiments as the polymer was cooled to liquid nitrogen temperatures. This insensitivity tends to support the assignment of the Raman peaks to each mode of deformation. Indeed, regarding the D* band, the polymer is a solid, so thermal stress can be transferred from the contracting matrix to the nanotubes by shear across the matrix−nanotube interface, resulting in axial compression and a spectral shift that is linear with strain (Figure 6). This linearity supports the strain identical assumption. Since the contracting matrix applies a hydrostatic stress, a shift associated with the tangential direction (i.e., the G band) would also be anticipated, since the contracting matrix forms a compressive envelope around the nanotubes. In this case though, the mechanical response is a consequence of a *stress* identical situation, where the stress in the nanotube wall is equal to the stress in the polymer. A likely explanation for the lack of shift for the G band is the following. Equation 2 can be modified by multiplying the modulus of the polymer matrix E_m on both sides of the equation to give

$$\sigma_m \approx E_m \alpha_m \Delta T \tag{3}$$

Although the matrix modulus is a temperature-dependent parameter, it becomes quickly apparent that the stress applied to the nanotubes is small ($E_m = 2.2$ GPa at room temperature and pressure), about 50 MPa at liquid nitrogen temperatures. A shift in the peak position of the G band is therefore not expected in the polymer experiments, especially when compared to the pressures imposed using the DAC (Figure 2). By the same rationale, if the D* band were responding to changes in tube diameter or intertube spacing due to matrix contraction (which corresponds to identical stresses in the tubes and the matrix), then similar trends would be expected in Figures 2 and 6, which is clearly not the case. Indeed, if in Figure 6 the D* band shift was plotted against stress instead of thermal strain, using eq 3, then the 20 cm^{-1} wavenumber shift would have to be attributed to the aforementionned 50 MPa contraction stress. Since this is far removed from the GPa range of pressures required in the DAC and the liquid experiments to attain the same Raman shift, we feel that the stress identical assumption is not appropriate. The Raman shift data therefore give direct information on the mechanical behavior of the nanotubes in that the D* band is linear with strain while the G band is linear with pressure or stress.

The deviation from linearity of the position of the G band with pressure is now addressed. Raman intensities will decrease with increasing diameter of tubes for all peaks except the G band,[25] and at the limit of infinite diameter, this is the only peak that does not have a nonvanishing intensity. It has also been suggested that the curved nature of the graphitic layers in nanotubes leads to an enhancement of the electron−photon coupling and thus to an increase in the intensity of the D band. Also, at large diameters the D band will approach the value for polycrystalline graphite before it finally disappears.[26] This implies that in the case of flattened tubes the D* band will vanish. It would also be expected that remaining peaks would exhibit a different shift−strain response, especially when it is considered that, owing to van der Waals forces, the inner walls can suddenly interact.[27] Since the deviation from linearity of the G band occurs around 2000 MPa, which is coincident with the vanishing D* peak and the weak intensity from the nanotube spectrum measured in water, it is proposed that a structural event has occurred, such as the flattening of the tubes. Flattening has been observed by transmission electron microscopy [28] and has also been initiated using an electron beam.[29] An approximate calculation can be used to determine the pressure p_c required to cause tube collapse. If the collapse is perfectly elastic, then continuum elasticity theory predicts[30]

$$p_c = \frac{2E}{(1-\nu^2)}\left(\frac{t}{d}\right)^3 \tag{4}$$

where E and ν are Young's modulus and Poisson's ratio of the nanotube wall and t and d are the wall thickness and diameter of the tube, respectively. If the modulus is taken as 5 TPa, the wall thickness as 0.066 nm, and Poisson's ratio as 0.19,[22] then for the mean tube diameter (1.1 nm), the predicted collapse pressure p_c is 2241 MPa. This value supports the hypothesis that the spectral data reflect changes in the nanotube structure.

If flattening has occurred, then the deformation seems to be reversible because the D* peak emerges above the baseline spectrum as the pressure is reduced to ambient pressure. The reversible nature of the shifted peak positions back to the peak position in air when the liquids were evaporated also corroborates that there was little permanent deformation. Such reversible deformation was not observed in the studies of Chopra et al.[29] because in their experiments the electron beam actually destroyed the tube structure. Energetic considerations have been used to predict the stability of flat, fully collapsed tubes with respect to the inflated counterpart.[28,31] A critical radius was predicted for single-wall nanotubes, which implies that for the tubes in our investigation, the inflated tube is more favorable than the collapsed tube; i.e., any collapsed tube will spontaneously reinflate once the collapsing pressure has been removed. TEM observations under such high pressures are presently not feasible, although work is in progress to ascertain whether liquid-induced collapse can be observed.

Conclusions

We have shown that high-pressure data are coincident with the shift of the D* peak position on immersion in liquids. This supports the hypothesis that the nanotubes are acting as molecular sensors and adds further validity to the compressive stress−strain curve. The G band position shows a linear dependence with pressure, and the D* peak shows a linear dependence with strain, supplying further evidence to assignment of these peaks to mechanical deformation modes. A decrease in the intensity of the D* peak was found to be coincident with a deviation from linearity of the G band position against pressure. A simple calculation to predict the collapse of nanotubes under hydrostatic pressures supports that flattening of the tubes has occurred.

Note Added in Proof. Recently, Ventkateswaran et al.[32] have reported high-pressure data where the pressure medium was a methanol/ethanol mixture (4:1 by volume). Their measurements show that the low-frequency breathing vibrational modes between 150 and 220 cm^{-1} disappear at 1500 MPa, about 500 MPa lower than the value reported in this paper. If the cohesive energy density of the methanol/ethanol mixture (838 MPa) is added to their pressure value, the pressures for the disappearance of the breathing modes from both studies are remarkably similar. This reinforces the proposed concordance between the cohesive energy density and hydrostatic pressure and supports the applicability of single-wall nanotubes as molecular sensors.

Acknowledgment. This project was supported in part by a grant from the Minerva Foundation and in part by the Israel Science Foundation founded by the Israel Academy of Sciences and Humanities. The referees are thanked for stimulating comments.

References and Notes

(1) Ijima, S.; Brabec, C.; Maiti, A.; Bernholc, J. *J. Chem. Phys.* **1996**, *104*, 2089.
(2) Treacy, M. M. J.; Ebbesen, T. W.; Gibson, J. M. *Nature* **1996**, *381*, 678.
(3) Overney, G.; Zhong, W.; Tomanek, Z. *Phys. D.* **1993**, *27*, 93.
(4) Robertson, D. H.; Brener, D. W.; Mintmire, J. W. *Phys. Rev. B* **1992**, *45*, 12592.
(5) Wagner, H. D.; Lourie, O.; Feldman, Y.; Tenne, R. *Appl. Phys. Lett.* **1998**, *72*, 188.
(6) Lourie, O.; Cox, D. M.; Wagner, H. D. *Phys. Rev. Lett.* **1998**, *81*, 1638.
(7) Tuinstra, F.; Koenig, J. L. *J. Chem. Phys.* **1970**, *53*, 1126.
(8) Lourie, O.; Wagner, H. D. *J. Mater. Res.* **1998**, *13*, 2418.
(9) Wood, J. R.; Wagner, H. D. *Phys. Rev. Lett.*, submitted.
(10) Rao, A. M.; Richter, E.; Bandow, S.; Chase, B.; Eklund, P. C.; Williams, K. A.; Fang, S.; Subbaswamy, K. R.; Menon, M.; Thess, A.; Smalley, R. E.; Dresselhaus, G.; Dresselhaus, M. S. *Science* **1997,** *275*, 187.
(11) Holden, J. M.; Zhou, P.; Bi, X.-X.; Eklund, P. C.; Bandow, S.; Jishi, R. A.; Das Chowdhury, K.; Dresselhaus, G.; Dresselhaus, M. S. *Chem. Phys. Lett.* **1994**, *220*, 186.
(12) Saito, R.; Takeya, T.; Kimura, T.; Dresselhaus, G.; Dresselhaus, M. S. *Phys. Rev. B* **1999**, *59*, 2388.
(13) Mernagh, T. P.; Cooney, R. P.; Johnson, R. H. *Carbon* **1984**, *22*, 39.
(14) Pimenta, M. A.; Marucci, A.; Empedoceles, S. A.; Bawendi, M. G.; Hanlon, E. B.; Rao, A. M.; Eklund, P. C.; Smalley, R. E.; Dresselhaus, G.; Dresselhaus, M. S. *Phys. Rev. B* **1998**, *58*, 16016.
(15) Glasstone, S. *Textbook of Physical Chemistry*, 2nd ed; D. Van Nostrand Co. Inc.: New York, 1946; pp 479−480.
(16) Grulke, E. A. In *Polymer Handbook*, 3rd ed; Brandrup, J., Immergut, E. H., Eds.; J. Wiley and Sons: New York, 1989; pp 519−559.
(17) Dunstan, D. J.; Scherrer, W. *Rev. Sci. Instrum.* **1988**, *59*, 627.
(18) Barnett, J. D.; Block, S.; Piermarini, G. *Rev. Sci. Instrum.* **1973**, *44*, 1.
(19) Hildebrand, J. H.; Scott, R. L. *The Solubility of Nonelectrolytes*, 3rd ed; Reinhold: New York, 1948; pp 401−402.
(20) Freitag, D.; Grigo, U.; Muller, P. R.; Nouvertne, W. In *Encyclopedia of Polymer Science and Engineering*; Kroschwitz, J. I., Ed.; Wiley: New York, 1986; pp 648−718.
(21) Van Krevelen, D. W. *Properties of Polymers*, 3rd ed; Elsevier Science Publishers: Amsterdam, 1990; pp 189−226.
(22) Yakobson, B. I.; Brabec, C. J.; Berholc, J. *Phys. Rev. Lett.* **1996**, *76*, 2511.
(23) Treloar, L. R. G. *The Physics of Rubber Elasticity*, 3rd ed; Oxford University Press: Oxford, 1975; pp 80−90.
(24) Krishnan, A.; Dujardin, E.; Ebbesen, T. W.; Yianilos, P. N.; Treacy, M. M. J. *Phys. Rev. B* **1998**, *58*, 14013.
(25) Jishi, R. A.; Venkataraman, L.; Dresselhaus, M. S.; Dresselhaus, G. *Chem. Phys. Lett.* **1993**, *209*, 77.
(26) Kastner, J.; Pichler, T.; Kuzmany, H.; Curran, S.; Blau, W.; Weldon, D. N.; Delamesiere, M.; Draper, S.; Zandbergen, H. *Chem. Phys. Lett.* **1994**, *221*, 53.
(27) Ruoff, R. S.; Tersoff, J.; Lorents, D. C.; Subramoney, S.; Chan, B. *Nature* **1993**, *364*, 514.
(28) Chopra, N. G.; Benedict, L.; Crespi, V.; Cohen, M.; Louie, S.; Zettl, A. *Nature* **1995**, *377*, 135.
(29) Chopra, N. G.; Ross, F. M.; Zettl, A. *Chem. Phys. Lett.* **1996**, *256*, 241.
(30) Timoshenko, S. *Theory of Elastic Stability*, 1st ed.; McGraw-Hill: New York, 1936; p 6.
(31) Benedict, L. X.; Chopra, N. S. Cohen, M. L.; Zettl, A.; Louie, S. G.; Crespi, V. H. *Chem. Phys. Lett.* **1998**, *286*, 490.
(32) Venkateswaran, U. D.; Rao, A. M.; Richter, E.; Menon, M.; Rinzle, A.; Smalley, R. E.; Eklund, P. C. *Phys. Rev. B* **1999**, *59*, 10928.